Dalton Transactions

ROYAL SOCIETY OF CHEMISTRY

PAPER

View Article Online
View Journal | View Issue

Cite this: *Dalton Trans.*, 2025, **54**, 13509

Theoretical study of the mechanisms of activation/deactivation of luminescence in a UiO-66 type sensor modified with Ln^{3+} (Eu and Tb) as dopant ions

Yoslainy Echevarria-Valdés,[a] Yoan Hidalgo-Rosa,[b,g] Eduardo Schott,[c] Manuel A. Treto-Suárez,[d] Dayán Páez-Hernández *[a,e] and Ximena Zarate*[f]

The luminescence properties of MOF-based materials have been improved by incorporating lanthanide ions (Ln^{3+}) *via* post-synthetic modifications (PSM). In this report, a quantum chemical theoretical protocol was carried out to elucidate the detection principle of the *turn-on* luminescence mechanism in a modified MOF labeled as Ln^{3+}@UiO-66-$(COOH)_2$ (Ln^{3+} = Eu^{3+} or Tb^{3+}). The MOF is composed of Zr_6-octahedron $\{[Zr_6(\mu_3\text{-}O)_4(\mu_3\text{-}OH)_4]^{12+}\}$ nodes; ligands (also called linkers) of 1,2,4,5-benzenetetracarboxylic acid (H_4btec); and Eu^{3+} and Tb^{3+} ions, which coordinate through the free carboxylate groups. The multi-configurational post-Hartree–Fock method *via* CASSCF/NEVPT2 calculations and the analysis of rate constants associated with radiative and nonradiative deactivations (k_F, k_P and k_{ISC}) were used to understand the photophysical processes governing the sensing mechanisms in the Ln^{3+}@UiO-66-$(COOH)_2$ sensor. The most likely sensitization channel is the population of the first excited triplet (T_1) state of the H_4btec linker through intersystem crossing ($S_1 \rightarrow T_1$), followed by energy transfer (ET) from H_4btec (T_1) to Eu^{3+} ($^5D_4$), followed by vibrational relaxation (VR) processes from the $^5D_4$ state to the $^5D_0$ (Eu^{3+}) state, producing radiative deactivation towards ^7F_J states and enhanced luminescence. Moreover, the Tb^{3+} ion was considered an alternative to Eu^{3+}. In this case, the results showed a similar sensitization channel in which energy transfer could occur, likely towards the $^5D_2$ state of Tb^{3+}. This theoretical protocol offers a powerful tool to investigate the photophysical properties of MOF-based systems doped with lanthanide ions.

Received 9th July 2025,
Accepted 8th August 2025

DOI: 10.1039/d5dt01615k

rsc.li/dalton

Introduction

Chemical sensors represent a viable alternative to traditional analytical methods, such as gas chromatography/mass spectrometry (GC/MS) and high-performance liquid chromatography (HPLC), for detecting and monitoring species hazardous to the environment and human health.[1–4] These systems have been employed for the *in situ* selective detection of biological species,[5,6] volatile organic compounds,[7] and metal ions.[8] Their ability to provide accurate health data in real time, combined with their portability and capacity for rapid and reliable detection of various analytes of interest,[9,10] has garnered significant attention. These advantages have driven their widespread application in multiple fields, including medicine, environmental monitoring, and industrial safety.[11] An ideal chemical sensor should exhibit key attributes such as stability, reversibility, and high selectivity,[1–4] the latter being essential for differentiating individual compounds within mixtures of unknown composition.[2,3]

Luminescent chemical systems have proven to be an effective alternative for the development of optical sensors.

[a]*Doctorado en Fisicoquímica Molecular, Facultad de Ciencias Exactas, Universidad Andrés Bello, República 275, Santiago 8370146, Chile. E-mail: dayan.paez@unab.cl*
[b]*Centro de Nanotecnología Aplicada, Facultad de Ciencias, Ingeniería y Tecnología, Universidad Mayor, Camino La Pirámide 5750, Huechuraba, Santiago 8580745, Chile*
[c]*Departamento de Química Inorgánica, Facultad de Química y de Farmacia, Centro de Energía UC, Centro de Investigación en Nanotecnología y Materiales Avanzados CIEN-UC, Pontificia Universidad Católica de Chile, Vicuña Mackenna 4860, Macul, 7820436 Santiago, Chile*
[d]*Departamento de Física y Química, Facultad de Ingeniería, IDETECO, Universidad Autónoma de Chile, Av. Alemania 01090, 4810101-Temuco, Chile*
[e]*Center of Applied Nanosciences (CANS), Universidad Andres Bello, Ave. República #275, 8370146 Santiago de Chile, Chile*
[f]*Instituto de Ciencias Aplicadas, Facultad de Ingeniería, Universidad Autónoma de Chile, Av. Pedro de Valdivia 425, Santiago, Chile. E-mail: ximena.zarate@uautonoma.cl*
[g]*Escuela de Ingeniería del Medio Ambiente y Sustentabilidad, Facultad de Ciencias, Ingeniería y Tecnología, Universidad Mayor, Camino La Pirámide 5750, Huechuraba, Santiago 8580745, Chile*

Luminescence-based techniques are particularly interesting since the variation in the intensity or energy of photons emitted after excitation can be related to the presence or absence of a particular analyte.[12–15] In this context, several studies have pointed to metal–organic frameworks (MOFs) as promising materials for chemical detection due to their exceptional optical and structural properties. These materials are porous and crystalline organic–inorganic hybrids. Their structure is composed of clusters or metal ions (nodes) coordinated with organic ligands (linkers), forming three-dimensional networks with unique chemical reactivity. Due to their organic and metallic composition, luminescence is produced through several types of mechanisms, including energy transfer (ET) and charge transfer (CT). CT can be categorized into linker-metal charge transfer (LMCT) or metal-linker charge transfer (MLCT).[16–18]

Among MOFs, the zirconium-based MOF UiO-66 stands out. It was named in honor of the University of Oslo, where it was first synthesized by Lillerud *et al.* in 2008.[19,20] UiO-66 is composed of secondary building units (SBUs) based on Zr_6-clusters, specifically $Zr_6(\mu_3\text{-}O)(\mu_3\text{-}OH)_4)(COO)_{12}^-$ octahedral SBUs, which are interconnected by twelve 1,4-benzenedicarboxylate (BDC) linkers. The remarkable chemical stability of UiO-66 under diverse conditions, including exposure to air, water, organic solvents, and elevated external pressures, can be attributed to the robust Zr–O bonds and high coordination number between the Zr_6-clusters and the BDC linkers.[21] This stability is a result of the high charge density and bond polarization of Zr^{4+} ions, which demonstrate a strong electron affinity when interacting with the oxygen atoms of the carboxylate groups in the BDC linkers.[22] This MOF demonstrates exceptional thermal and hydrolytic stability,[23] rendering it highly suitable for practical applications, such as chemical sensing, across diverse environments.[24] A distinctive characteristic of these materials is their capacity to enhance optical properties by strategically integrating functional groups[25] or metal ions[26] into their frameworks. This modification results in a material that is isostructural to UiO-66, maintaining its inherent chemical and physical properties, while significantly boosting its optical performance. UiO-66 exhibits several properties that make it promising for the detection of a wide range of analytes, including target molecules such as amyloid-β (Aβ) (1–42) monomers,[27] volatile organic compounds (VOCs),[28] and dimethyl methylphosphonate (DMMP),[29] and metal ions.[30] Among the studied sensor materials, MOFs are a very interesting type that possess an important advantage over other classes of chemical sensors. For instance, their exceptional properties have led researchers to explore post-synthetic modification techniques (PSM) to obtain new materials, modifying many of their original properties without altering their topology.[9,31–33] This approach has become an important area of research, as it offers the possibility of introducing functional groups into the pores of MOFs, including species such as anions and cations, achieving an improvement in the structural stability of MOFs and introducing the desired properties into the material.[34–37]

Experimental and theoretical studies have investigated the electronic structures of UiO-66-type MOFs.[38–41] Research employing density of states (DOS) analysis[40] and electron paramagnetic resonance spectroscopy (EPR)[38] have indicated that electron transitions between ligands and metals have a low probability. These materials, which include both substituted and unsubstituted BDC linkers, suggest that the optical (absorption and emission) properties arise from the building components due to the linkers (conjugated organic ligands). DOS calculations for UiO-66(Zr) have shown that the lowest unoccupied metal orbital of Zr 4d is positioned approximately 2.0 eV above the lowest unoccupied linker orbital, highlighting the inefficient linker-to-metal charge transfer (LMCT) process.[41] This is characteristic of secondary building units (SBUs) based on closed-shell metal-ion complexes.[13]

A new generation of L-MOFs are those functionalized with lanthanide (Ln) ions (Ln@MOF) through PSM to activate the emission properties of the material and generate new emission signals centered on the lanthanide ions.[32,33,42,43] The improvements in the luminescent properties of these Ln ion-modified materials are the main attraction, which is due to the sharp line emissions, high color purity, high luminescence quantum yield and large Stokes shifts, attributed to the 4f–4f transitions and relativistic effects of Ln ions.[44–46]

The functionalization of UiO-66 with Ln(III) ions, referred to as Ln(III)@UiO-66, has emerged as a promising platform to develop luminescent chemical sensors for detecting metal ions.[47] This is attributed to the exceptional structural properties and chemical stability of UiO-66, combined with the remarkable luminescent properties of Ln(III) ions. For UiO-66, it has been reported that the light absorption depends on the linker, and for Ln(III)@UiO-66, the sensitization and emission pathways involve a linker that absorbs light in the UV region and transfers energy from its excited electronic state to the resonance level of the Ln(III) ions.[22,48–50] Upon interaction with an analyte, several phenomena can occur that affect the luminescence behavior: the analyte may quench the emission by introducing non-radiative decay pathways, modify the energy levels of the linker and thereby disrupt the energy transfer mechanism, or, in some cases, enhance the emission by stabilizing the excited states or facilitating more efficient energy transfer.[4,51–53] Another mechanism of sensing recently investigated for Ln(III)@UiO-66 sensors is the exchange of the emitted center (Ln^{3+}) in the coordination environment of the antenna ligand by the analyte.[50] This process quenches luminescence (*turn-off* sensing) by locking the sensitization path between ISC and ligand-to-metal energy transfer due to substitution of the Ln^{3+} ions. These luminescence modulations form the basis for detecting and quantifying the presence of specific analytes using Ln(III)@UiO-66 as an optical sensor.

For the specific case of compounds that present lanthanide Ln(III) ions in their structure, the most relevant properties that support many of the applications of these compounds originate from symmetry-forbidden 4f–4f transitions. However, these transitions exhibit very weak absorption, which results

in very weak luminescence. Their luminescence arises from a sensitization process carried out by ET through a suitable organic linker to the Ln ions, which is called the "antenna effect".[55–57] The process requires ISC ($S_1 \rightarrow T_1$) in the linker, with a $\Delta E(S_1 \rightarrow T_1)$ of ~5000 cm^{-1} (Reinhoudt's rule) to ensure efficient ISC.[58] This ISC will show a large rate if the transition involves a change in the type of molecular orbitals (El-Sayed rules).[59,60] Thus, to efficiently sensitize Ln ions, the T_1 energy should be higher than the resonance energy of Ln, with ΔE ($T_1 \rightarrow$ Ln) ~ 2500–4000 cm^{-1} (Latva's rule).[61] In this regard, it is important to consider the structure of antenna linkers that act as good sensitizers, which is a critical point in the development of good Ln(III) compounds and a valid elucidation of the energy transfer pathways, which is essential for accurate determination of the electronic states of the lanthanide fragment.[55,57,62,63]

Accurate and fine computational approaches have been rigorously applied by our group for the study of MOFs with Ln in their nodes. In this regard, Zarate *et al.*[14] carried out theoretical procedures, *via* quantum chemical computations, to elucidate the detection principle of the *turn-off* luminescence mechanism of an Eu-based metal–organic framework sensor (Eu-MOF). The analyte in this study was the nitroaromatic compound aniline. Specifically, the energy transfer channels that operate in this MOF, as well as the mechanism of luminescence quenching by interaction with the analyte, were investigated using well-known and accurate multiconfigurational *ab initio* methods along with TD-DFT. A detailed study of the sensitization pathway from the linker (antenna) to the lanthanide was accomplished. It starts with the intersystem crossing (ISC) from the first excited singlet (S_1) to the first excited triplet (T_1) electronic states of the linker, with subsequent energy transfer to the $^5D_0$ state of Eu^{3+} followed by the emission to the ground multiplet ^7F_J. In the same framework, Zarate *et al.*[64] employed computational quantum chemistry methods to demonstrate the importance of the host–guest interaction simulations and the rate constants of the radiative and nonradiative processes, to understand the sensing mechanism in the Ln-MOF sensors; in this case, a sensor with Tb^{3+}.

The computational protocol developed by our group[14,52,65] has proven to be a valuable tool for studying luminescent MOFs modified with lanthanide ions (Ln@MOFs). This methodology allows for a rigorous analysis of the activation and deactivation mechanisms responsible for lanthanide-centered luminescence within these materials. This protocol was successfully applied in a previous study by our group, in which we studied an analogous system, Eu@UiO-66(DPA), designed as a selective *turn-off* luminescent sensor for Hg^{2+} ions.[54] In that study, the MOF incorporated 2,6-pyridinedicarboxylic acid (DPA) as an antenna ligand, which allowed us to elucidate how the substitution of Eu^{3+} with Hg^{2+} affected the electronic structure of the system and caused the suppression of emission. Based on this methodology, the present work applies the same theoretical framework to investigate a different MOF platform.

In this paper, the system of interest is a modified MOF labeled as Eu^{3+}@UiO-66-$(COOH)_2$, which is composed of nodes of Zr_6-octahedron $\{[Zr_6(\mu_3\text{-}O)_4(\mu_3\text{-}OH)_4]^{12+}\}$, linkers of 1,2,4,5-benzenetetracarboxylic acid (H_4btec), and Eu(III), which is coordinated through the free carboxylate groups, forming a rigid coordination network, as reported by Ji-Na Hao *et al.*[52] (Fig. 1). The structural difference presented by this MOF implies that the detection mechanisms are intrinsically different from the systems recently studied by our research group, which is relevant from the point of view of its practical application. Although the system investigated in this work includes Eu^{3+} ions as the emitting center, the theoretical prediction of the photophysical behavior when Eu^{3+} is replaced with Tb^{3+} is also explored for the first time, with the aim of evaluating its potential performance in optical sensors. This study focuses on a systematic comparison of the luminescence sensitization mechanisms of both ions (Eu^{3+} and Tb^{3+}) incorporated into the UiO-66-$(COOH)_2$ structure, an aspect that was not addressed in previous research recently carried out by our research group, which focused exclusively on Eu^{3+}. This comparative approach allowed the optical response of the material to be optimized, revealing that the incorporation of Tb^{3+} significantly improves the luminescent efficiency of the system, highlighting its potential in the design of advanced optical sensors and light-emitting devices.

Computational details

A representative cluster model, corresponding to a finite fragment of the extended UiO-66, was constructed by truncating the crystalline structure derived from the experimental crystal data available in the Cambridge Crystallographic Data Centre (CCDC 1018045).[66] This procedure was performed due to the large size of the MOF, considering the particularities of the system that represents the structure of interest.[52,67,68] This methodology is based primarily on the fact that these materials exhibit a unique electronic structure with highly localized electronic states.[67–69] In the theoretical study reported here, UiO-66-$(COOH)_2$ was truncated to a fragment constituted by the Zr_6-octahedron $\{[Zr_6(\mu_3\text{-}O)_4(\mu_3\text{-}OH)_4]^{12+}\}$ node, four linkers of 1,2,4,5-benzenetetracarboxylic acid (H_4btec) and eight truncated linkers, as can be seen in Fig. 2a. Afterwards the Lanthanide (Ln^{3+}) was coordinated as a doping species, which we refer to as Ln^{3+}@UiO-66-$(COOH)_2$ (Fig. 2b). In this work, we have also considered the potential sensitization of luminescence for the Tb^{3+} ion because it shares a similar electronic structure to Eu^{3+} in terms of electrons and holes. In previous work, the sensitization of these ions by similar antennas has been successfully studied using the fragmentation scheme described above.[55,57,63,70,71]

Geometry optimizations of the ground state (S_0) of both systems, UiO-66-$(COOH)_2$ and Ln^{3+}@UiO-66-$(COOH)_2$, including for the latter the coordination sphere of lanthanide, were carried out using density functional theory (DFT), with the ORCA 5.0.3 software package.[72] Generalized Gradient Approximation (GGA) Becke-Perdew (BP86)[73] exchange–correlation functional was employed together the basis set, triple-ζ valence with one sets of polarization functions, def2-TZVP[74] for all atoms except for Eu and Tb which were computed with

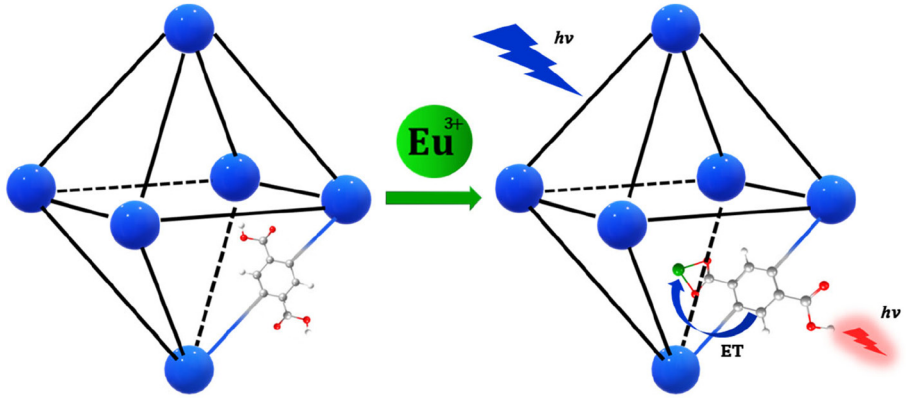

Fig. 1 Simplified scheme showing the increase in light emission by sensitization from the linker to the inserted Eu^{3+} ion.

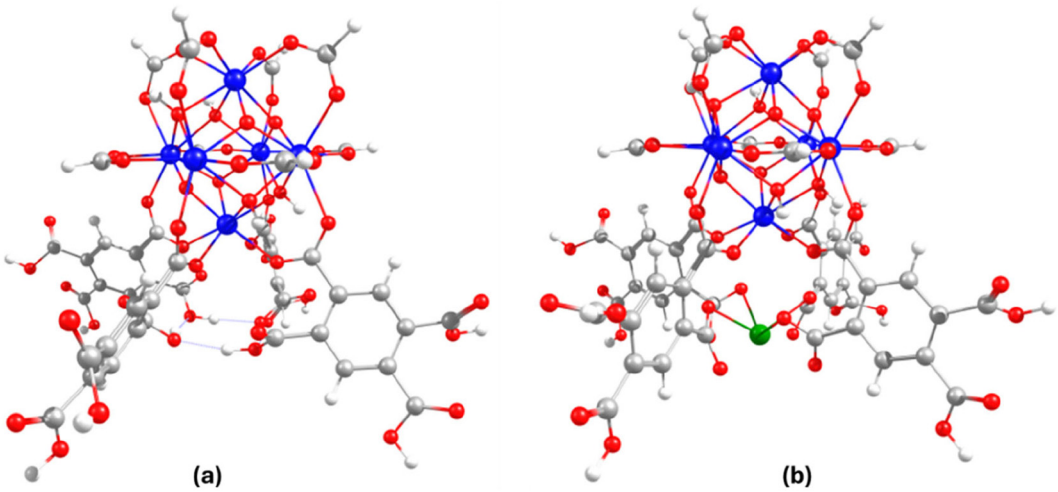

Fig. 2 Optimized geometry of the truncated systems at the BP86/def2-TZVP theoretical level: (a) UiO-66-$(COOH)_2$ and (b) Ln^{3+}@UiO-66-$(COOH)_2$ (Ln^{3+} = Eu^{3+} or Tb^{3+}).

the DKH optimized SARC with TZVP quality.[75–78] The structure of the T_1 state of the UiO-66-$(COOH)_2$ system was optimized at the same level of theory.

In the second stage of this work, a study of the optical properties related to light absorption of the UiO-66-$(COOH)_2$ and Ln^{3+}@UiO-66-$(COOH)_2$ systems was carried out, using the time-dependent DFT (TD-DFT) approach as implemented in the ORCA 5.0.3 software package.[72] The polarized triple-ζ basis set (TZV) def2-TZVP[74] was used with the hybrid-GGA Perdew–Burke–Ernzerhof (PBE0).[79] The RIJCOSX approximation was used to accelerate the SCF calculation by the combination of the RIJ method for the Coulomb term with the "chain of spheres" COSX approximation and their respective auxiliary basis set for computation of two-electron integrals.[80]

Starting from the optimized structure in the excited state T_1 of the UiO-66-$(COOH)_2$ system, the emission energies were assessed to analyze the optical properties through the time-dependent DFT (TD-DFT) approach, using the hybrid exchange and correlation functional, Perdew–Burke–Ernzerhof (PBE0)[79] *via* the ORCA 5.0.3 software package.[72] Furthermore, the polarized triple-ζ basis set (TZV) quality def2-TZVP[74] was used for the C, H, N, and O atoms.

To elucidate the sensitization and emission pathways, the theoretical procedure reported by Beltrán-Leiva *et al.*[55,57,63] was applied. The wave function that describes the ground- and excited-states of the Eu-fragment and the linker fragment was obtained through CASSCF methods.[81] A dynamic correlation was also included by means of the *n*-electron valence state perturbation theory (NEVPT2) approach.[82] In this approximation, for trivalent Eu^{3+}, all possible distributions of six unpaired electrons among the seven 4f active orbitals CAS (6,7) were considered, which included 7 septuplets, 40 quintuplets, 30 triples, and 20 singles.[63] Similarly, for Tb^{3+}, the active space considered was CAS (8,7), including the same number of states in each multiplicity. The same level of theory was used to obtain the energy values of the S_0, S_1, and T_1 electronic states

for the $[H_4btec]^-$ linker. For this fragment, an active space of ten electrons in ten orbitals CAS (10, 10) was used, all of them with π character.

We analyzed the excited-state dynamics of the antenna linker $[H_4btec]^-$ to establish the activation/deactivation channels of the photophysical processes that introduce Eu^{3+} as a doping species. The calculations of the excited state dynamics of the antenna linker were performed based on the strategy (fragmentation scheme) proposed by M. J. Beltrán-Leiva *et al.*[57] for organometallic complexes based on lanthanides. This procedure involved the geometry optimizations and frequency calculations of the ground state and the first excited states (singlet and triplet) of the linkers of the Ln^{3+}@UiO-66-$(COOH)_2$ system. Using the ORCA ESD module of the ORCA 5.0.3 software package,[72] we calculated the intersystem crossing (ISC), phosphorescence, and fluorescence rates, which we will refer to as k_{ISC}, k_P, and k_F, respectively.[57,62] The energy transfer rates were determined using time-dependent density functional theory (TD-DFT) calculations in conjunction with the LUMPAC software package[83] (**https://lumpac.pro.br/**).

Due to the availability of experimental results for the Eu^{3+} system, the discussion will focus on this ion in the following section, leaving the discussion of Tb^{3+} for the luminescence sensitization section.

Results and discussion

Optical properties and structure

The structural models proposed for both systems, in general, successfully reproduce the geometrical parameters. The computed and experimental bond lengths for [Zr–O(linker)], [Zr–O(μ_3-OH)] and [Zr–O(μ_3-O)] displayed a good correlation. The theoretical magnitudes are 2.22 Å, 2.24 Å and 2.09 Å, respectively, and the reported experimental data are 2.23 Å, 2.25 Å and 2.06 Å, respectively, for this MOF.[84]

The vertical excitation energies also agree with the experimental values reported for both systems, as can be seen in Table 1. In the computed absorption spectrum of UiO-66-$(COOH)_2$ (see Fig. S1a in the SI), absorption bands centered at 294 and 295 nm appear, which are attributed to several configurations with vertical transitions from the frontier molecular orbitals. These correspond to π–π* transitions of the linker (H_4btec), which is in good agreement with the reported experimental excitation wavelength at around 350 nm.[52] The molecular orbitals involved in these electronic transitions can be seen in Fig. S2. The difference in energy is within the error range of the TD-DFT method (roughly 50 nm).[64,85] In case of the Eu^{3+}@UiO-66-$(COOH)_2$, the simulated absorption spectrum displays absorption bands centered at 296 and 299 nm, which correspond to π–π* transitions (see Fig. S1b and Fig. S3), and is in great accordance with the reported experimental absorption wavelength at 322 nm.[52] Small variations in the position of the bands towards higher wavelength values are observed because the coordination of the Eu^{3+} ion produces polarization effects on the linker, resulting in an increase in the electron cloud and a stabilization in energy.[55]

It is interesting to note that, according to the results obtained by TDDFT calculations, the presence of the lanthanide ion does not notably influence the absorption spectrum. The absorption bands are localized on the linker, since the molecular orbitals involved in the $S_0 \rightarrow S_1$ electronic transition remain mostly located on the π system of the organic linker, without a relevant participation of the Eu^{3+} ion. This indicates that the adsorption process is mainly governed by the electronic structure of the antenna ligand, independently of the lanthanide center. It is known that the metal–ligand interaction in these complexes is ionic in nature, and the internal character of the 4f shell prevents any metal–ligand charge transfer. The ligand–metal transfer is likewise impeded because the vacant orbitals of the metal are usually sufficiently high in energy and cannot be accessed by electrons of the ligand.

Consequently, no direct electronic transfer between the lanthanide ion and the ligand occurs, which validates the approach of considering the ligand model in isolation in the CASSCF/NEVPT2 multiconfigurational calculations, since the sensitization of Ln^{3+} occurs by nonradiative energy transfer from the ligand triplet state (T_1) to the emissive levels of the lanthanide ion, and not by direct coupling *via* charge transfer.

Regarding the emission, UiO-66-$(COOH)_2$ shows a broad emission band, arising from the π–π* transitions of the linkers

Table 1 Electronic transitions for the absorption and emission processes of the linkers at the PBE0/def2-TZVP theoretical level for UiO-66-$(COOH)_2$ and Eu^{3+}@UiO-66-$(COOH)_2$[a]

System	λ_{max} (nm)	f	Active MO	Assignment
UiO-66-$(COOH)_2$ absorption	295	0.03	H−1 → L+3	$\pi(L^{H,btec}) \rightarrow \pi^*(L^{H,btec})$
	294	0.03	H−1 → L	$\pi(L^{H,btec}) \rightarrow \pi^*(L^{H,btec})$
	294	0.02	H−1 → L+1	$\pi(L^{H,btec}) \rightarrow \pi^*(L^{H,btec})$
Eu^{3+}@UiO-66-$(COOH)_2$ Absorption	299	0.01	H−4 → L+1	$\pi(L^{H,btec}) \rightarrow \pi^*(L^{H,btec})$
	296	0.03	H−5 → L+1	$\pi(L^{H,btec}) \rightarrow \pi^*(L^{H,btec})$
UiO-66-$(COOH)_2$ Emission	**338**	**0.05**	**L → H**	$\boldsymbol{\pi(L^{H,btec}) \rightarrow \pi^*(L^{H,btec})}$

[a] H is HOMO, L is LUMO. Abbreviations: HOMO (highest energy occupied orbital); LUMO (unoccupied orbital of lower energy); MO (molecular orbital). Experimental values for absorption bands of UiO-66-$(COOH)_2$ and Eu^{3+}@UiO-66-$(COOH)_2$ are 350 and 322 nm (ref. 52) and emission for UiO-66-$(COOH)_2$ is observed at 393 nm.[53]

(H_4btec).[52] TD-DFT results show a π–π* transition centered on the linker, which is composed of the frontier molecular orbitals shown in Fig. S4. The emission band obtained theoretically is centered at 338 nm, which is in good agreement with the experimental emission wavelength reported for the isolated ligand at around 393 nm.[53] The difference in energy is within the error range of the TD-DFT method (approximately 50 nm).[64,85]

Sensitization and emission pathways

The sensitization and emission pathways in MOF modified with lanthanides (Ln@MOF) involve a step in which energy is transferred from the T_1 electronic state of the linker to a resonant level of the Ln^{3+} ions, [Linker (T_1) → Ln^{3+}]. This ET process is possible because spin–orbit coupling (SOC) induces a mixture of states of different multiplicities of the metal.[14,55] In this regard, Crosby *et al.*[86] point out that the energy of the T_1 electronic state of the linker respects the 4f excited states energy of the lanthanide ion, as well as the vibrational coupling between these states, allowing efficient sensitization to the lanthanide. In addition, Latva *et al.*[61] emphasize that the accurate estimation of the T_1 electronic state energy of the antenna plays a key role in determining the most likely sensitization mechanism, with this energy being in the range of 2500–4000 cm^{-1}.

To gain a deeper understanding of the most probable sensitization and emission mechanisms, further *ab initio* calculations were performed to correctly determine the electronic states of the linkers and lanthanide ions involved in the sensitization mechanism.

Based on the foregoing and considering that the absorption in the Eu^{3+}@UiO-66-$(COOH)_2$ system is linker-centered H_4btec, we applied the fragmentation scheme reported by Beltrán-Leiva *et al.*[57,63] in 2017 for lanthanide(III) complexes. Based on this methodology, we separate the systems into two fragments, one of which consists of the lanthanide moiety, while the other constitutes the linker according to the system (see Fig. S5 in the SI). For the theoretical treatment of the europium fragments, due to the ionic nature of the metal–ligand interaction and the internal nature of the 4f shell, a crystal field model, considering the first coordination sphere and simplifying the rest of the ligand, is enough to correctly describe the electronic states of the lanthanide ion.[57,63] In this sense, the CASSCF approximation in combination with the NEVPT2 method is a powerful methodology to treat the electronic static and dynamic correlation effects, respectively.

Based on the above and in accordance with the results obtained through TD-DFT, the $[H_4btec]^-$ fragment is responsible for the photon absorption; therefore, it was studied to evaluate the sensitization channels in the Eu^{3+}@UiO-66-$(COOH)_2$ system. The $[H_4btec]^-$ fragment was treated at the same theoretical level as for the europium fragment (CAS (6,7) SCF/NEVPT2), considering an active space of ten orbitals CAS (10,10) all π character. In Table 2, the S_1 electronic state, with a 63% contribution of the configuration (π → π*) at 39 853 cm^{-1}, and the T_1 electronic state, with a 72% contribution of the same configuration at 32 148 cm^{-1}, correspond to the excited states of the antenna linker $[H_4btec]^-$. These results are analyzed in detail by means of CASSCF/NEVPT2 calculations, which provide information on the active orbitals involved and their fractional occupancy. This occupancy, which can be complete or intermediate, is in an optimal range, suggesting that the selected orbitals are adequate to correctly describe the electronic behavior of the molecule.[55,57,81] Thus, the correct distribution of electrons in the active orbitals allows an accurate description of the excited states observed, as listed in the SI Table S1, confirming the validity of the results obtained for the S_1 and T_1 electronic states in the framework of the theoretical calculations.

Table 2 Singlet and triplet energy states and the most important configurations obtained from a CAS (10,10) SCF/NEVPT2 calculation for the linker $[H_4btec]^-$ fragment

		Energy, cm^{-1}			
States		CASSCF	NEVPT2	Weight (%)	Configuration
Singlet	S_1	36 989	39 853	28	$\pi^2\pi^2\pi^2\pi^1\pi^2\pi^1\pi^0\pi^0\pi^0\pi^0$
				21	$\pi^2\pi^2\pi^2\pi^2\pi^1\pi^0\pi^1\pi^0\pi^0\pi^0$
				14	$\pi^2\pi^2\pi^2\pi^2\pi^1\pi^1\pi^0\pi^0\pi^0\pi^0$
	S_2	53 455	42 698	41	$\pi^2\pi^2\pi^2\pi^2\pi^1\pi^1\pi^0\pi^0\pi^0\pi^0$
				17	$\pi^2\pi^2\pi^2\pi^1\pi^2\pi^1\pi^0\pi^0\pi^0\pi^0$
Triplet	T_1	28 078	32 148	43	$\pi^2\pi^2\pi^2\pi^2\pi^1\pi^1\pi^0\pi^0\pi^0\pi^0$
				17	$\pi^2\pi^2\pi^2\pi^1\pi^2\pi^1\pi^0\pi^0\pi^0\pi^0$
				12	$\pi^2\pi^2\pi^2\pi^1\pi^2\pi^0\pi^1\pi^0\pi^0\pi^0$
	T_2	36 246	36 338	25	$\pi^2\pi^2\pi^2\pi^2\pi^1\pi^1\pi^0\pi^0\pi^0\pi^0$
				25	$\pi^2\pi^2\pi^2\pi^1\pi^2\pi^1\pi^0\pi^0\pi^0\pi^0$
				12	$\pi^2\pi^2\pi^2\pi^1\pi^2\pi^0\pi^1\pi^0\pi^0\pi^0$

All the values reported in the table were computed by means of CASSCF and NEVPT2 using the ORCA 5.0.3 software package.[72]

According to Reinhoudt's rule,[58] the intersystem crossing (ISC, S_1 → T_1) is most efficient when the energy difference between the first singlet and triplet excited states is around 5000 cm^{-1}. However, this rule is empirical and should be understood as an optimal range rather than an absolute limit. Therefore, the efficient occurrence of the ISC process is not ruled out when the energy difference is outside this range, since it depends on the specific characteristics of the system under study. In case of the Eu^{3+}@UiO-66-$(COOH)_2$ system, the calculated energy difference between the S_1 and T_1 states is 7704 cm^{-1}, a value larger than the one proposed by that rule. Despite this, experimental evidence reports the characteristic emission bands of the Eu^{3+} ion, indicating that the population of the T_1 state and the subsequent energy transfer to the Eu^{3+} ion occur efficiently.[52] To validate this hypothesis beyond an empirical estimate, we further consider the strong spin–orbit coupling (SOC) effect characteristic of Ln^{3+} ions in this type of material, which induces a significant mixing of electronic states with different multiplicities. This phenomenon alters the electronic levels distribution and favors the coupling between singlet and triplet states, facilitating an efficient intersystem crossing (ISC), even when the S_1-T_1 energy difference is

outside the empirically proposed optimal range. Furthermore, the excited state dynamics of the $[H_4btec]^-$ antenna ligand were studied to perform a more rigorous quantitative analysis. This approach allowed us to determine the rate constants associated with the photophysical deactivation processes (fluorescence (k_F) and intersystem conversion (k_{ISC})), thus providing a solid quantitative basis for assessing the efficiency of the proposed sensitization mechanism. The obtained results show that the ISC channel is favored over fluorescence. In particular, the rate constant for the ISC process ($S_1 \rightarrow T_1$) was 4.43×10^8 s^{-1}, being three orders of magnitude higher than the k_F fluorescence constant ($S_1 \rightarrow S_0$), which was found to be 3.18×10^5 s^{-1} (see Fig. 3). These results confirm that, although the S_1–T_1 energy difference is above the empirical optimal range, the ISC mechanism remains highly efficient, constituting the predominant pathway for the population of the T_1 state and subsequent sensitization of the Eu^{3+} ion.

The proposed structural model for the europium fragment and the selection of the active space in the CAS (6,7) SCF/NEVPT2 calculations have proven to be effective in accurately reproducing the energy values of the Eu^{3+} ion electronic states, which are in agreement with the experimental values reported for this lanthanide.[87] The obtained results, reflected in the SI Table S2, show the selected active orbitals and their respective fractional occupancy numbers, which are in the optimal range.[55,57,81] This fit in orbital occupancy indicates that the orbitals were adequately chosen to describe the excited states of the system, ensuring that the theoretical calculations faithfully reflect the electronic behavior of the europium fragment and provide an accurate representation of its electronic properties.

According to the CAS(6,7)SCF/NEVPT2 calculations, the S_1 electronic state $[H_4btec]^-$ is situated in energy well above the electronic states of the lanthanide, for this reason the probability of an ET process from this state can be considerably reduced, but this is not the case for the electronic state T_1 $[H_4btec]^-$, which is situated 3589 cm^{-1} above the electronic state $^5D_4$ (28 558 cm^{-1}) of the Eu^{3+} ion. Therefore, the most likely mechanism is an ET channel from the T_1 $[H_4btec]^-$ to the $^5D_4$ electronic state of Eu^{3+}, with this energy gap being in good agreement with the optimal range, to sensitize Eu^{3+} ion luminescence based on Latva's rule[61] ΔE (Linker $T_1 \rightarrow Ln^{3+}$) ~ 2500–4000 cm^{-1}. Moreover, as shown in Fig. 3, the k_P rate is 1.11×10^3 s^{-1}, which means that the lifetime of the T_1 $[H_4btec]^-$ electronic state favors ET channels from the $[H_4btec]^-$ (T_1) $\rightarrow$ Eu^{3+} ($^5D_4$) electronic state, from where $^5D_4$ vibrational relaxation processes occur until populating the electronic state $^5D_0$ electronic state (18 637 cm^{-1}) from which radiative deactivation to ^7F_J states occurs, resulting in the luminescence turn-on of Eu^{3+}@UiO-66-$(COOH)_2$ system (see Fig. 3).

Based on the previously discussed ISC process, favored by the presence of a heavy metal and the S_1–T_1 energy difference, it is correct to assume that the energy transfer mechanism can also occur for the Tb^{3+} ion. In fact, even when the energy difference between the $^5D_4$ (~23 600 cm^{-1}) emissive state of Tb^{3+} and the triplet state of the antenna is out of the range set by Latva's rule, the energy transfer mechanism would favor higher energy electronic states. The energy difference between the T_1 electronic state of the antenna ligand and the $^5D_2$ (~29 300 cm^{-1}) excited state of the ion is ~2800 cm^{-1}. From these results, it is possible to conclude that a mechanism like

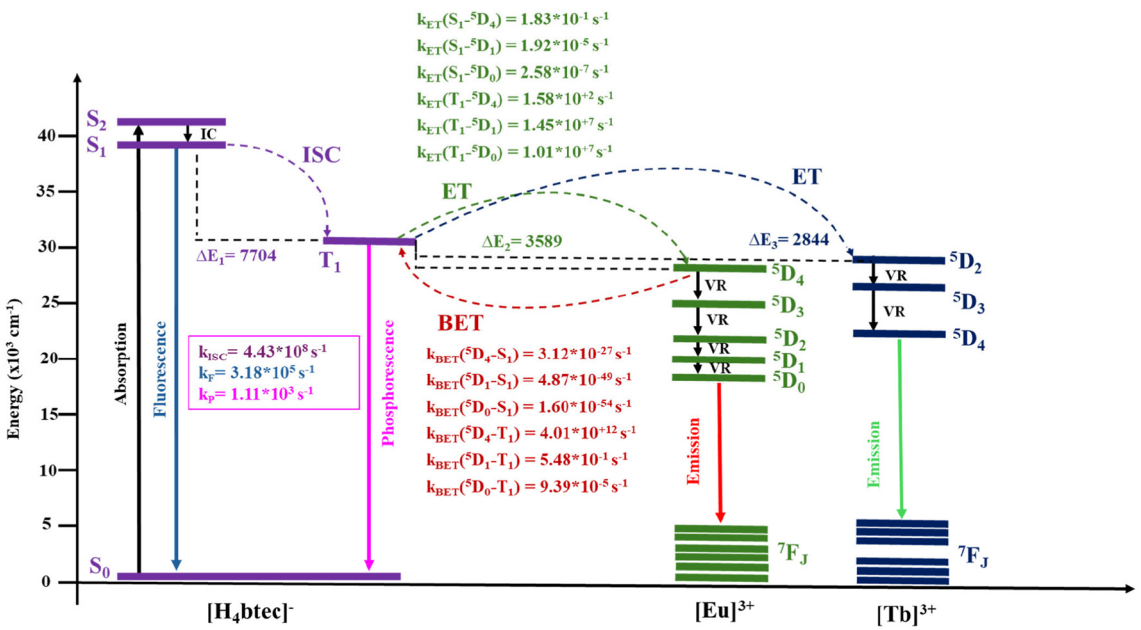

Fig. 3 Diagram of energy levels illustrating the most probable pathways for sensitization and emission for the Ln^{3+}@UiO-66-$(COOH)_2$ (Ln^{3+} = Eu^{3+} or Tb^{3+}) system. Intersystem crossing, phosphorescence, fluorescence, energy transfer, and back energy transfer rates are represented by k_{ISC}, k_P, k_F, k_{ET} and k_{BET}, respectively.

that described for Eu^{3+} will be possible for the Tb^{3+} ion, with sensitization occurring most likely through the $^5D_2$ electronic state (see Fig. 3).

While empirical rules, such as Latva's rule, provide general guidelines on the efficiency of sensitization based on the energy differences between the triplet state of the ligand and the excited states of the lanthanide ion, they should not be interpreted as absolute limits. In this study, such rules serve as a starting point to suggest the feasibility of the ET process. However, to quantitatively validate this hypothesis, ET and back energy transfer (BET) rates were calculated using LUMPAC software[83] for the Eu^{3+} doped system. Thus, this analysis was not performed for the material containing the Tb^{3+} ion as a dopant species, due to the absence of reported experimental data for this system. The obtained values allow a more precise determination of the efficiency of the sensitization process, overcoming the limitations of a purely qualitative or empirical evaluation.

As shown in Fig. 3, ET rates (k_{ET}) are distributed in a range from 10^{-7} to 10^{7} s^{-1}. This behavior reflects the negative values of k_{ET}, corresponding to the electronic state S_1, indicating unfavorable or even nonexistent energy transfer from that state to the Eu^{3+} ion. In contrast, the k_{ET} values associated with the T_1 state suggest that this state does allow a viable and efficient energy transfer channel. Consequently, the T_1 state of the ligand is identified as the primary sensitization pathway.

In contrast, the S_1 state is found to be inadequate for ET processes, which is attributed to its energy mismatch and the low probability of resonant coupling with the electronic levels of the Eu^{3+} ion. The k_{ET} (S_1–$^5D_4$) = 1.83×10^{-1} s^{-1}, k_{ET} (S_1–$^5D_1$) = 1.92×10^{-5} s^{-1} and k_{ET} (S_1–$^5D_0$) = 2.58×10^{-7} s^{-1} are lower than the corresponding values for probable ET from the T_1 electronic state, with k_{ET} (T_1–$^5D_4$) = 1.58×10^{2} s^{-1}, k_{ET} (T_1–$^5D_1$) = 1.45×10^{7} s^{-1} and k_{ET} (T_1–$^5D_0$) = 1.01×10^{7} s^{-1}. This result supports the hypothesis raised from the empirical rules and sustains the conclusion that the sensitization process is feasible, being quantitatively more efficient from the triplet state of the ligand. In particular, the magnitude of the k_{ET} rates from the T_1 state (on the order of 10^2–10^7 s^{-1}) evidences that this channel represents the dominant pathway for the luminescence activation process in the Eu^{3+}@UiO-66-$(COOH)_2$ system.

Based on the BET values rates: k_{BET} ($^5D_4$–T_1) = 4.01×10^{12} s^{-1}, k_{BET} ($^5D_1$–T_1) = 5.48×10^{-1} s^{-1} and k_{BET} ($^5D_0$–T_1) = 9.39×10^{-5} s^{-1}, the high value of k_{BET} from the $^5D_4$ state to the T_1 state could imply a competitive effect favoring non-radiative processes, negatively affecting the emission quantum yield. However, this phenomenon does not invalidate the efficiency of the sensitization mechanism, since the k_{BET} values for the lower emissive states of Eu^{3+}, $^5D_1$ and $^5D_0$, turn out to be significantly lower. This suggests that, once the lower emissive levels are reached, radiative emission can proceed efficiently, without considerable energy loss to the triplet state of the ligand. Thus, these results support the experimental observations of luminescence in the system, demonstrating that, despite the possible unfavorable effect of k_{BET} from the $^5D_4$ level, the emission process is still viable and effective. Likewise, the BET rates k_{BET} ($^5D_4$–S_1) = 3.12×10^{-27} s^{-1}, k_{BET} ($^5D_1$–S_1) = 4.87×10^{-49} s^{-1} and k_{BET} ($^5D_0$–S_1) = 1.60×10^{-54} s^{-1} confirm the negligible role of the BET process for the electronic state S_1 in this system.

To design luminescent sensors based on MOFs, it is crucial to emphasize the central role played by the Ln^{3+} ion in the mechanism of luminescence activation and deactivation. The efficiency of the sensitization process depends directly on the proper energy transfer from the triplet state (T_1) of the antenna ligand to the emissive electronic levels of the Ln^{3+} ion, such as the $^5D_0$ (Eu^{3+}) or $^5D_4$ (Tb^{3+}) states. This adequate transfer refers to an optimal energy match between the T_1 state of the ligand and the excited levels of the Ln^{3+} ion, where the energy difference must be within a range that favors coupling without inducing unwanted processes such as backward energy transfer (BET) or non-radiative relaxation. Various empirical rules, such as Latva's rule,[61] suggest that effective coupling occurs when this difference is 2500–4000 cm^{-1}. Furthermore, the modulation of the emission efficiency is conditioned by the ability of the Ln^{3+} to compete effectively against non-radiative deactivation routes, such as vibrational relaxation (VR) and backward energy transfer (BET). Therefore, the Ln^{3+} ions not only act as an emissive center but also regulate the viability of the entire photoactive process, positioning itself as the key element in the design of highly efficient luminescent materials.

Conclusions

In this investigation, TD-DFT and multireference calculations were used to evaluate the potential energy transfer mechanism and to assess the rate constants associated with the radiative and nonradiative deactivations involved in the sensitization process. The results help to explain the photophysical processes that govern the sensing mechanisms in the Eu^{3+}@UiO-66-$(COOH)_2$ sensor and demonstrate the potential extension to Tb^{3+}. In this work, truncated versions of the extended structures of UiO-66-$(COOH)_2$ and Ln^{3+}@UiO-66-$(COOH)_2$ (Ln^{3+} = Eu^{3+} or Tb^{3+}) systems were constructed as finite structural models that successfully reproduced the geometric parameters and photophysical properties of the systems. The most probable sensitization channels for the Ln^{3+}@UiO-66-$(COOH)_2$ system were described based on CASSCF/NEVPT2 calculations and by examining the antenna excited state dynamics, taking into account intersystem crossing (k_{ISC}), fluorescence (k_F), and phosphorescence (k_P) rate constants. The results indicate that the most likely sensitization pathway involves the population of the T_1 electronic state of the $[H_4btec]^-$ linker through the ISC process ($S_1 \rightarrow T_1$) and subsequent ET of the $[H_4btec]^-$ (T_1) $\rightarrow$ Eu^{3+} ($^5D_4$) linker, from where VR processes occur until the $^5D_0$ electronic state is populated, from which radiative deactivation to ^7F_J states occurs, resulting in luminescence in this system. Similarly, it was established that the possible sensitization pathway of Tb^{3+}

could occur through an energy transfer to the $^5D_2$ state of the ion.

The results obtained using LUMPAC confirm that ET is the dominant sensitization mechanism in the Eu^{3+}@UiO-66-$(COOH)_2$ system, despite possible competition from the BET process from higher excited levels ($^5D_4$). The low probability of BET from the $^5D_1$ and $^5D_0$ emissive states ensures efficient emission, which validates the proposed mechanism and supports the efficiency of the sensor.

Finally, the theoretical protocol employed provides a powerful tool to investigate various lanthanide ion-modified MOF systems, elucidating the sensitization and emission pathways that govern the sensing mechanisms and guiding the design of such chemical sensors. With this work, we can also conclude that a reliable theoretical protocol has been established for simulating the optical properties of lanthanide-doped MOFs based on the construction of a truncated but representative model of the extended system, followed by the application of a fragmentation scheme to determine the sensitization mechanism by the antenna effect. The application of this protocol to a significant number of systems of this nature has proven to be useful not only as a complement to experimental research but also as a predictive tool to guide such work.

Conflicts of interest

There are no conflicts to declare.

Data availability

The data supporting this article have been included as part of the SI.

Calculated UV-vis spectra and assignment of the transition for both UiO-66-$(COOH)_2$ and Eu@UiO-66-$(COOH)_2$ models and the active orbitals considered for the antenna and lanthanide ion in the CASSCF/NEVPT2 calculations are presented. See DOI: **https://doi.org/10.1039/d5dt01615k**.

Acknowledgements

The authors thank the PhD Program in Molecular Physical Chemistry from University Andrés Bello, the financial support from ANID/Chile under Doctoral Fellowship 21240110 and Projects FONDECYT 1231194, FONDECYT 1241917 FONDECYT 1220442, FONDECYT Postdoctoral 3210271, FONDECYT Postdoctoral 3230141, Anillos de Ciencia y Tecnología ACT210057. ANID/FONDAP/1523A0006. This material is based upon work supported by the Air Force Office of Scientific Research under award number FA8655-25-1-8759.

References

1 S. W. T. Iii, G. D. Joly and T. M. Swager, Chemical Sensors Based on Amplifying Fluorescent Conjugated Polymers, *Chem. Rev.*, 2007, **107**, 1339–1386.
2 C. Sensors, Introduction : Chemical Sensors, *Chem. Rev.*, 2019, **119**, 9–10, DOI: **10.1021/acs.chemrev.8b00764**.
3 H. Adam, S. Geab and F. Ingman, Chemical Sensors Definitions and Classification, *Pure Appl. Chem.*, 1991, **63**(9), 1247–1250.
4 Y. Shu, Q. Ye, T. Dai, Q. Xu and X. Hu, Encapsulation of Luminescent Guests to Construct Luminescent Metal-Organic Frameworks for Chemical Sensing, *ACS Sens.*, 2021, **6**(3), 641–658, DOI: **10.1021/acssensors.0c02562**.
5 X. Guo, L. Zhou, X. Liu, G. Tan, F. Yuan, A. Nezamzadeh-ejhieh, N. Qi, J. Liu and Y. Peng, Fluorescence Detection Platform of Metal-Organic Frameworks for Biomarkers, *Colloids Surf., B*, 2023, **229**, 113455, DOI: **10.1016/j.colsurfb.2023.113455**.
6 Y. Jin and B. Yan, A Bi-Functionalized Metal-Organic Framework Based on N-Methylation and Eu 3+ Post-Synthetic Modification for Highly Sensitive Detection of 4-Ami Nophenol (4-AP), a Biomarker for Aniline in Urine, *Talanta*, 2021, **227**(2020), 122209, DOI: **10.1016/j.talanta.2021.122209**.
7 C. J. Balzer, M. R. Armstrong, B. Shan and B. Mu, Composite MOF Mixture as Volatile Organic Compound Sensor – A New Approach to LMOF Sensors, *Mater. Lett.*, 2017, **190**, 33–36, DOI: **10.1016/j.matlet.2016.12.111**.
8 L. Prodi, F. Bolletta, M. Montalti, V. Selmi and I. Bologna, Luminescent Chemosensors for Transition Metal Ions, *Coord. Chem. Rev.*, 2000, **205**, 59–83.
9 J. N. Hao and B. Yan, Highly Sensitive and Selective Fluorescent Probe for Ag+ Based on a Eu3+ Post-Functionalized Metal-Organic Framework in Aqueous Media, *J. Mater. Chem. A*, 2014, **2**(42), 18018–18025, DOI: **10.1039/c4ta03990d**.
10 M. A. Treto-Suárez, E. Schott, K. M. Ulecia, B. D. Koivisto, Y. Hidalgo-Rosa, D. Páez-Hernández and X. Zarate, Understanding the Deactivating/Activating Mechanisms in Three Optical Chemosensors Based on Crown Ether with Na+/K+ Selectivity Using Quantum Chemical Tools, *ChemPhysChem*, 2022, **23**(17), e202200188, DOI: **10.1002/cphc.202200188**.
11 T. Elias Abi-Ramia Silva, F. Burisch and A. T. Güntner, Gas Sensing for Space: Health and Environmental Monitoring, *TrAC, Trends Anal. Chem.*, 2024, **177**, 117790, DOI: **10.1016/j.trac.2024.117790**.
12 J. Jin, J. Xue, Y. Liu, G. Yang and Y. Y. Wang, Recent Progresses in Luminescent Metal-Organic Frameworks (LMOFs) as Sensors for the Detection of Anions and Cations in Aqueous Solution, *Dalton Trans.*, 2021, **50**(6), 1950–1972, DOI: **10.1039/d0dt03930f**.
13 Y. Hidalgo-Rosa, M. A. Treto-Suárez, E. Schott, X. Zarate and D. Páez-Hernández, Sensing Mechanism Elucidation of a Chemosensor Based on a Metal-Organic Framework

Selective to Explosive Aromatic Compounds, *Int. J. Quantum Chem.*, 2020, **120**(23), 1–11, DOI: 10.1002/qua.26404.

14 Y. Hidalgo-Rosa, M. A. Treto-Suárez, E. Schott, X. Zarate and D. Páez-Hernández, Sensing Mechanism Elucidation of a Europium(III) Metal–Organic Framework Selective to Aniline: A Theoretical Insight by Means of Multiconfigurational Calculations, *J. Comput. Chem.*, 2020, **41**(22), 1956–1964, DOI: 10.1002/jcc.26365.

15 Y. Zhang, S. Yuan, G. Day, X. Wang, X. Yang and H. C. Zhou, Luminescent Sensors Based on Metal-Organic Frameworks, *Coord. Chem. Rev.*, 2018, **354**, 28–45, DOI: 10.1016/j.ccr.2017.06.007.

16 W. P. Lustig, S. Mukherjee, N. D. Rudd, A. V. Desai, J. Li and S. K. Ghosh, Metal-Organic Frameworks: Functional Luminescent and Photonic Materials for Sensing Applications, *Chem. Soc. Rev.*, 2017, **46**(11), 3242–3285, DOI: 10.1039/c6cs00930a.

17 P. H. M. Andrade, C. Volkringer, T. Loiseau, A. Tejeda, M. Hureau and A. Moissette, Band Gap Analysis in MOF Materials: Distinguishing Direct and Indirect Transitions Using UV–Vis Spectroscopy, *Appl. Mater. Today*, 2024, **37**, 102094, DOI: 10.1016/j.apmt.2024.102094.

18 Z. Hu, B. J. Deibert and J. Li, Luminescent Metal–Organic Frameworks for Chemical Sensing and Explosive Detection, *Chem. Soc. Rev.*, 2014, **43**(16), 5815–5840, DOI: 10.1039/c4cs00010b.

19 J. H. Cavka, S. Jakobsen, U. Olsbye, N. Guillou, C. Lamberti, S. Bordiga and K. P. Lillerud, A New Zirconium Inorganic Building Brick Forming Metal Organic Frameworks with Exceptional Stability, *J. Am. Chem. Soc.*, 2008, **130**(42), 13850–13851, DOI: 10.1021/ja8057953.

20 J. Winarta, B. Shan, S. M. McIntyre, L. Ye, C. Wang, J. Liu and B. Mu, A Decade of UiO-66 Research: A Historic Review of Dynamic Structure, Synthesis Mechanisms, and Characterization Techniques of an Archetypal Metal-Organic Framework, *Cryst. Growth Des.*, 2020, **20**(2), 1347–1362, DOI: 10.1021/acs.cgd.9b00955.

21 F. Ahmadijokani, H. Molavi, M. Rezakazemi, S. Tajahmadi, A. Bahi, F. Ko, T. M. Aminabhavi, J. R. Li and M. Arjmand, UiO-66 Metal–Organic Frameworks in Water Treatment: A Critical Review, *Prog. Mater. Sci.*, 2022, **125**, 100904, DOI: 10.1016/j.pmatsci.2021.100904.

22 L. Yang, Y. L. Liu, X. X. Ji, C. G. Liu, Y. Fu and F. Ye, A Novel Luminescent Sensor Based on Tb@UiO-66 for Highly Detecting Sm3+ and Teflubenzuron, *J. Taiwan Inst. Chem. Eng.*, 2021, **126**, 173–181, DOI: 10.1016/j.jtice.2021.07.028.

23 R. D'Amato, A. Donnadio, M. Carta, C. Sangregorio, D. Tiana, R. Vivani, M. Taddei and F. Costantino, Water-Based Synthesis and Enhanced CO 2 Capture Performance of Perfluorinated Cerium-Based Metal-Organic Frameworks with UiO-66 and MIL-140 Topology, *ACS Sustainable Chem. Eng.*, 2019, 7(1), 394–402, DOI: 10.1021/acssuschemeng.8b03765.

24 S. Ghosh, A. Das and S. Biswas, A Functionalized UiO-66 MOF Acting as a Luminescent Chemosensor for Selective and Sensitive Turn-on Detection of Superoxide and Acetylacetone, *Microporous Mesoporous Mater.*, 2021, **323**, 111251, DOI: 10.1016/j.micromeso.2021.111251.

25 G. Mohammadi Ziarani, F. Moradi-Chaleshtori, M. Mirhosseyni, M. Feizi-Dehnayebi and A. Badiei, Functionalizing UiO-66-NH2 by 4-chloro-3-Formylcoumarin, as an Optical Chemosensor of Al3+ and F− and Its Computational Studies, *J. Mol. Struct.*, 2025, **1325**, 140947, DOI: 10.1016/j.molstruc.2024.140947.

26 T. Du, J. Wang, L. Zhang, S. C. Wang, C. Yang, L. Xie, Z. Liu, Y. Ni, X. H. Xie, J. Sun, W. Zhang and J. Wang, Missing-Linker Engineering of Eu(III)-Doped UiO-MOF for Enhanced Detection of Heavy Metal Ions, *Chem. Eng. J.*, 2022, **431**, 134050, DOI: 10.1016/j.cej.2021.134050.

27 Q. Fan, J. Wang, J. M. Biazik, S. Geng, F. Mazur, Y. Li, P. C. Ke and R. Chandrawati, UiO-66-NH2 Metal-Organic Framework for the Detection of Alzheimer's Biomarker Aβ (1–42), *ACS Appl. Bio Mater.*, 2024, **7**(1), 182–192, DOI: 10.1021/acsabm.3c00768.

28 S. Okur, T. Hashem, E. Bogdanova, P. Hodapp, L. Heinke, S. Bräse and C. Wöll, Optimized Detection of Volatile Organic Compounds Utilizing Durable and Selective Arrays of Tailored UiO-66-X SURMOF Sensors, *ACS Sens.*, 2024, **9**(2), 622–630, DOI: 10.1021/acssensors.3c01575.

29 I. Stassen, B. Bueken, H. Reinsch, J. F. M. Oudenhoven, D. Wouters, J. Hajek, V. Van Speybroeck, N. Stock, P. M. Vereecken, R. Van Schaijk, D. De Vos and R. Ameloot, Towards Metal-Organic Framework Based Field Effect Chemical Sensors: UiO-66-NH2 for Nerve Agent Detection, *Chem. Sci.*, 2016, **7**(9), 5827–5832, DOI: 10.1039/c6sc00987e.

30 A. A. Ansari, A. M. Khan, M. A. S. Salem and A. S. Bhat, Synthesis and Characterization of Ni@UiO-66 Metal-Organic Framework for Fluorescence Detection of Heavy Metal Ions in the Aqueous Phase, *Mater. Chem. Phys.*, 2024, **318**, 129245, DOI: 10.1016/j.matchemphys.2024.129245.

31 S. Mandal, S. Natarajan, P. Mani and A. Pankajakshan, Post-Synthetic Modification of Metal–Organic Frameworks Toward Applications, *Adv. Funct. Mater.*, 2021, **31**(4), 1–22, DOI: 10.1002/adfm.202006291.

32 J. N. Hao and B. Yan, Ag+-Sensitized Lanthanide Luminescence in Ln3+ Post-Functionalized Metal-Organic Frameworks and Ag+ Sensing, *J. Mater. Chem. A*, 2015, **3**(9), 4788–4792, DOI: 10.1039/c4ta06462c.

33 J. N. Hao and B. Yan, Ln3+ Post-Functionalized Metal-Organic Frameworks for Color Tunable Emission and Highly Sensitive Sensing of Toxic Anions and Small Molecules, *New J. Chem.*, 2016, **40**(5), 4654–4661, DOI: 10.1039/c5nj03419a.

34 S. Mandal, S. Natarajan, P. Mani and A. Pankajakshan, Post-Synthetic Modification of Metal – Organic Frameworks Toward Applications, *Adv. Funct. Mater.*, 2021, **31**(4), 22, DOI: 10.1002/adfm.202006291.

35 J. Xiao, J. Liu, M. Liu, G. Ji and Z. Liu, Fabrication of a Luminescence-Silent System Based on a Post-Synthetic Modification Cd-MOFs: A Highly Selective and Sensitive

Turn-on Luminescent Probe for Ascorbic Acid Detection, *Inorg. Chem.*, 2019, **58**(9), 6167–6174, DOI: **10.1021/acs.inorgchem.9b00420**.

36 S. M. Cohen, Postsynthetic Methods for the Functionalization of Metal-Organic Frameworks, *Chem. Rev.*, 2012, **112**(2), 970–1000, DOI: **10.1021/cr200179u**.

37 Y. Cui, J. Zhang, H. He and G. Qian, Photonic Functional Metal-Organic Frameworks, *Chem. Soc. Rev.*, 2018, **47**(15), 5740–5785, DOI: **10.1039/c7cs00879a**.

38 M. A. Nasalevich, C. H. Hendon, J. G. Santaclara, K. Svane, B. Van Der Linden, S. L. Veber, M. V. Fedin, A. J. Houtepen, M. A. Van Der Veen, F. Kapteijn, A. Walsh and J. Gascon, Electronic Origins of Photocatalytic Activity in D0 Metal Organic Frameworks, *Sci. Rep.*, 2016, **6**, 23676, DOI: **10.1038/srep23676**.

39 E. Flage-Larsen, A. Røyset, J. H. Cavka and K. Thorshaug, Band Gap Modulations in UiO Metal-Organic Frameworks, *J. Phys. Chem. C*, 2013, **117**(40), 20610–20616, DOI: **10.1021/jp405335q**.

40 A. De Vos, K. Hendrickx, P. Van Der Voort, V. Van Speybroeck and K. Lejaeghere, Missing Linkers: An Alternative Pathway to UiO-66 Electronic Structure Engineering, *Chem. Mater.*, 2017, **29**(7), 3006–3019, DOI: **10.1021/acs.chemmater.6b05444**.

41 X. P. Wu, L. Gagliardi and D. G. Truhlar, Cerium Metal-Organic Framework for Photocatalysis, *J. Am. Chem. Soc.*, 2018, **140**(25), 7904–7912, DOI: **10.1021/jacs.8b03613**.

42 H. Zheng, X. Lian, S. Qin and B. Yan, Novel "Turn-On" Fluorescent Probe for Highly Selectively Sensing Fluoride in Aqueous Solution Based on Tb 3+ -Functionalized Metal – Organic Frameworks, *ACS Omega*, 2018, **3**(10), 12513–12519, DOI: **10.1021/acsomega.8b02134**.

43 X. Xu and B. Yan, Eu(III)-Functionalized MIL-124 as Fluorescent Probe for Highly Selectively Sensing Ions and Organic Small Molecules Especially for Fe(III) and Fe(II), *ACS Appl. Mater. Interfaces*, 2015, **7**, 721–729, DOI: **10.1021/am5070409**.

44 B. Zhao, Lanthanide-Based Metal–Organic Frameworks as Luminescent Probes, *Dalton Trans.*, 2016, **45**(45), 18003–18017, DOI: **10.1039/c6dt02213h**.

45 Y. Cui, J. Zhang, C. Banglin and Q. Guodong, Lanthanide Metal-Organic Frameworks for Luminescent Applications, *Handb. Phys. Chem. Rare Earths*, 2016, **50**(243), 243–268, DOI: **10.1016/bs.hpcre.2016.04.001**.

46 S. N. Zhao, G. Wang, D. Poelman and P. Van Der Voort, Luminescent Lanthanide MOFs: A Unique Platform for Chemical Sensing, *Materials*, 2018, **11**(4), 1–26, DOI: **10.3390/ma11040572**.

47 H. Sohrabi, S. Ghasemzadeh, S. Shakib, M. R. Majidi, A. Razmjou, Y. Yoon and A. Khataee, Metal-Organic Framework-Based Biosensing Platforms for the Sensitive Determination of Trace Elements and Heavy Metals: A Comprehensive Review, *Ind. Eng. Chem. Res.*, 2023, **62**(11), 4611–4627, DOI: **10.1021/acs.iecr.2c03011**.

48 Z. Zhang, L. Liu, T. Zhang and H. Tang, Efficient Eu3+-Integrated UiO-66 Probe for Ratiometric Fluorescence Sensing of Styrene and Cyclohexanone, *ACS Appl. Mater. Interfaces*, 2023, **15**(15), 18982–18991, DOI: **10.1021/acsami.3c01204**.

49 L. Li, L. L. Zhang, J. Zou, J. Zou, L. Y. Duan, Y. Gao, G. Peng, X. Huang and L. Lu, Dual-Emissive Europium Doped UiO-66-Based Ratiometric Light-up Biosensor for Highly Sensitive Detection of Histidinemia Biomarker, *Anal. Chim. Acta*, 2024, **1290**, 342202, DOI: **10.1016/j.aca.2024.342202**.

50 Z. Xiaoxiong, Z. Wenjun, L. Cuiliu, Q. Xiaohong and Z. Chengyu, Eu3+-Postdoped UIO-66-Type Metal-Organic Framework as a Luminescent Sensor for Hg2+ Detection in Aqueous Media, *Inorg. Chem.*, 2019, **58**(6), 3910–3915, DOI: **10.1021/acs.inorgchem.8b03555**.

51 X. Zhang, L. Fang, K. Jiang, H. He, Y. Yang, Y. Cui, B. Li and G. Qian, Nanoscale Fluorescent Metal – Organic Framework Composites as a Logic Platform for Potential Diagnosis of Asthma, *Biosens. Bioelectron.*, 2019, **130**, 65–72, DOI: **10.1016/j.bios.2019.01.011**.

52 J. N. Hao and B. Yan, A Water-Stable Lanthanide-Functionalized MOF as a Highly Selective and Sensitive Fluorescent Probe for Cd2+, *Chem. Commun.*, 2015, **51**(36), 7737–7740, DOI: **10.1039/c5cc01430a**.

53 X. Zhang, Q. Hu, T. Xia, J. Zhang, Y. Yang, Y. Cui, B. Chen and G. Qian, Turn-on and Ratiometric Luminescent Sensing of Hydrogen Sulfide Based on Metal – Organic Frameworks, *ACS Appl. Mater. Interfaces*, 2016, **8**, 32259–32265, DOI: **10.1021/acsami.6b12118**.

54 Y. Hidalgo-Rosa, Y. Echevarria-Valdés, M. Saavedra-Torres, D. Páez-Hernández, E. Schott and X. Zarate, Quantum Chemical Elucidation of the Luminescence Mechanism in a Europium(III) Co-Doped UiO-66 Chemosensor Selective to Mercury(II), *Dalton Trans.*, 2025, **54**(16), 6623–6636, DOI: **10.1039/d4dt03285c**.

55 M. J. Beltrán-Leiva, D. Páez-Hernández and R. Arratia-Pérez, Theoretical Determination of Energy Transfer Processes and Influence of Symmetry in Lanthanide(III) Complexes: Methodological Considerations, *Inorg. Chem.*, 2018, **57**(9), 5120–5132, DOI: **10.1021/acs.inorgchem.8b00159**.

56 S. I. Weissman, Intramolecular Energy Transfer The Fluorescence of Complexes of Europium, *J. Chem. Phys.*, 1942, **10**, 214–217, DOI: **10.1063/1.1723709**.

57 M. J. Beltrán-Leiva, E. Solis-Céspedes and D. Páez-Hernández, The Role of the Excited State Dynamic of the Antenna Ligand in the Lanthanide Sensitization Mechanism, *Dalton Trans.*, 2020, **49**(22), 7444–7450, DOI: **10.1039/d0dt01132k**.

58 L. Yu, L. Feng, L. Xiong, S. Li, Q. Xu, X. Pan and Y. Xiao, Rational Design of Dual-Emission Lanthanide Metal-Organic Framework for Visual Alkaline Phosphatase Activity Assay, *ACS Appl. Mater. Interfaces*, 2021, **13**(10), 11646–11656, DOI: **10.1021/acsami.1c00134**.

59 B. Y. M. Kasha, Characterization of Electronic Tran- Sitions in Complex Molecules, in *Complex Molecules*, 1950, pp. 14–19.

60 M. A. Elsayed, Spin—Orbit Coupling and the Radiationless Processes in Nitrogen Heterocyclics, *Chem. Phys.*, 1963, **38**, 2834–2838, DOI: **10.1063/1.1733610**.
61 M. Latva, H. Takalob, V. Mukkala, C. Matachescuc, J. C. Rodriguez-ubisd and J. Kankarea, Correlation between the Lowest Triplet State Energy Level of the Ligand and Lanthanide(III) Luminescence Quantum Yield, *J. Lumin.*, 1997, **75**, 149–169.
62 J. J. Santoyo-Flores and D. Páez-Hernández, Theoretical Study of 8-Hydroxyquinoline Derivatives as Potential Antennas in Lanthanide Complexes: Photophysical Properties and Elucidation of Energy Transfer Pathways, *Int. J. Quantum Chem.*, 2022, **122**(10), 2022e26880, DOI: **10.1002/qua.26880**.
63 M. J. Beltrán-Leiva, P. Cantero-López, C. Zúñiga, A. Bulhões-Figueira, D. Páez-Hernández and R. Arratia-Pérez, Theoretical Method for an Accurate Elucidation of Energy Transfer Pathways in Europium(III) Complexes with Dipyridophenazine (Dppz) Ligand: One More Step in the Study of the Molecular Antenna Effect, *Inorg Chem.*, 2017, **56**(15), 9200–9208, DOI: **10.1021/acs.inorgchem.7b01221**.
64 Y. Hidalgo-Rosa, K. Mena-Ulecia, M. A. Treto-Suárez, E. Schott, D. Páez-Hernández and X. Zarate, Expanding the Knowledge of the Selective-Sensing Mechanism of Nitro Compounds by Luminescent Terbium Metal-Organic Frameworks through Multiconfigurational Ab Initio Calculations, *J. Phys. Chem. A*, 2022, **126**(39), 7040–7050, DOI: **10.1021/acs.jpca.2c05468**.
65 Y. Hidalgo-Rosa, K. Mena-Ulecia, M. A. Treto-Suárez, E. Schott, D. Páez-Hernández and X. Zarate, Insights into the Selective Sensing Mechanism of a Luminescent Cd (II)-Based MOF Chemosensor toward NACs: Roles of the Host–Guest Interactions and PET Processes, *J. Mater. Sci.*, 2021, **56**(24), 13684–13704, DOI: **10.1007/s10853-021-06196-3**.
66 S. Øien, D. Wragg, H. Reinsch, S. Svelle, S. Bordiga, C. Lamberti and K. P. Lillerud, Detailed Structure Analysis of Atomic Positions and Defects in Zirconium Metal-Organic Frameworks, *Cryst. Growth Des.*, 2014, **14**(11), 5370–5372, DOI: **10.1021/cg501386j**.
67 J. L. Mancuso, A. M. Mroz, K. N. Le and C. H. Hendon, Electronic Structure Modeling of Metal-Organic Frameworks, *Chem. Rev.*, 2020, **120**(16), 8641–8715, DOI: **10.1021/acs.chemrev.0c00148**.
68 S. O. Odoh, C. J. Cramer, D. G. Truhlar and L. Gagliardi, Quantum-Chemical Characterization of the Properties and Reactivities of Metal-Organic Frameworks., *Chem. Rev.*, 2015, **115**(12), 6051–6111, DOI: **10.1021/cr500551h**.
69 V. Bernales, M. A. Ortuño, D. G. Truhlar, C. J. Cramer and L. Gagliardi, Computational Design of Functionalized Metal-Organic Framework Nodes for Catalysis, *ACS Cent. Sci.*, 2018, **4**(1), 5–19, DOI: **10.1021/acscentsci.7b00500**.
70 Z. Abbas, S. Dasari, M. J. Beltrán-Leiva, P. Cantero-López, D. Páez-Hernández, R. Arratia-Pérez, R. J. Butcher and A. K. Patra, Luminescent Europium(III) and Terbium(III) Complexes of β-Diketonate and Substituted Terpyridine Ligands: Synthesis, Crystal Structures and Elucidation of Energy Transfer Pathways, *New J. Chem.*, 2019, **43**(38), 15139–15152, DOI: **10.1039/c9nj02838b**.
71 Y. Hidalgo-Rosa, J. Santoyo-Flores, M. A. Treto-Suárez, E. Schott, D. Páez-Hernández and X. Zarate, Tuning the Sensitization Pathway T1→5DJ in Eu-Based MOF through Modification of the Antenna Ligand. A Theoretical Approach via Multiconfigurational Quantum Calculations, *J. Lumin.*, 2023, **260**, 119896, DOI: **10.1016/j.jlumin.2023.119896**.
72 F. Neese, The ORCA Program System, *Wiley Interdiscip. Rev.:Comput. Mol. Sci.*, 2012, **2**(1), 73–78, DOI: **10.1002/wcms.81**.
73 J. P. Perdew and Y. Wang, *Phys. Rev. B*, 1986, **33**, 8800.
74 F. Weigend and R. Ahlrichs, Balanced Basis Sets of Split Valence, Triple Zeta Valence and Quadruple Zeta Valence Quality for H to Rn: Design and Assessment of Accuracy, *Phys. Chem. Chem. Phys.*, 2005, **7**(18), 3297–3305, DOI: **10.1039/b508541a**.
75 M. Dolg, H. Stoll, A. Savin and H. Preuss, *Energy-Adjusted Pseudopotentials for the Rare Earth Elements*, Springer-Verlag, 1989, vol. 75.
76 D. A. Pantazis and F. Neese, All-Electron Scalar Relativistic Basis Sets for the Actinides, *J. Chem. Theory Comput.*, 2011, **7**(3), 677–684, DOI: **10.1021/ct100736b**.
77 J. M. L. Martin and A. Sundermann, Correlation Consistent Valence Basis Sets for Use with the Stuttgart-Dresden-Bonn Relativistic Effective Core Potentials: The Atoms Ga-Kr and In-Xe, *J. Chem. Phys.*, 2001, **114**(8), 3408–3420, DOI: **10.1063/1.1337864**.
78 X. Cao, M. Dolg and X. Cao, Valence Basis Sets for Relativistic Energy-Consistent Small-Core Lanthanide Pseudopotentials, *Chem. Phys.*, 2001, **115**(16), 7348–7355, DOI: **10.1063/1.1406535**.
79 C. Lee, W. Yang and R. G. Parr, Development of the Colic-Salvetti Correlation-Energy Formula into a Functional of the Electron Density, *Phys. Rev. B:Condens. Matter Mater. Phys.*, 1988, **37**(2), 785–789.
80 G. L. Stoychev, A. A. Auer and F. Neese, Automatic Generation of Auxiliary Basis Sets, *J. Chem. Theory Comput.*, 2017, **13**(2), 554–562, DOI: **10.1021/acs.jctc.6b01041**.
81 B. O. Roos, P. R. Taylor and P. E. M. Siegbahn, *A Complete Active Space SCF Method (CASSCF) Using a Density Matrix Formulated Super-Ci Approach*, 1980, vol. 48.
82 C. Angeli, R. Cimiraglia, S. Evangelisti, T. Leininger and J. P. Malrieu, Introduction of N-Electron Valence States for Multireference Perturbation Theory, *J. Chem. Phys.*, 2001, **114**(23), 10252, DOI: **10.1063/1.1361246**.
83 J. D. L. Dutra, T. D. Bispo and R. O. Freire, LUMPAC Lanthanide Luminescence Software: Efficient and User Friendly, *J. Comput. Chem.*, 2014, **35**(10), 772–775, DOI: **10.1002/jcc.23542**.
84 S. Øien, D. Wragg, H. Reinsch, S. Svelle, S. Bordiga, C. Lamberti and K. P. Lillerud, Detailed Structure Analysis of

Atomic Positions and Defects in Zirconium Metal – Organic Frameworks, *Cryst. Growth Des.*, 2014, **14**, 5370–5372.
85 J. P. Perdew, M. Ernzerhof and K. Burke, Rationale for Mixing Exact Exchange with Density Functional Approximations, *J. Chem. Phys.*, 1996, **105**(22), 9982–9985, DOI: **10.1063/1.472933**.
86 G. A. Crosby, R. E. Whan and R. M. Alire, Intramolecular Energy Transfer in Rare Earth Chelates. Role of the Triplet State, *J. Chem. Phys.*, 1961, **34**(3), 743–748, DOI: **10.1063/1.1731670**.
87 Y. Cui, Y. Yue, G. Qian and B. Chen, Luminescent Functional Metal–Organic Frameworks, *Chem. Rev.*, 2012, **112**(2), 1126–1162, DOI: **10.1021/cr200101d**.